Check for updates

Geophysical Research Letters

RESEARCH LETTER
10.1029/2024GL111311

Chronology, Local Stratigraphy, and Foreign Ejecta Materials at the Chang'e-6 Landing Site: Constraints on the Provenance of Samples Returned From the Moon's Farside

Luyuan Xu[1,2], Le Qiao[3], Minggang Xie[4], Yiran Wang[5], Meng-Hua Zhu[1], and Jianguo Yan[2]

[1]State Key Laboratory of Lunar and Planetary Sciences, Macau University of Science and Technology, Macau, China, [2]State Key Laboratory of Information Engineering in Surveying, Mapping and Remote Sensing, Wuhan University, Wuhan, China, [3]Shandong Key Laboratory of Optical Astronomy and Solar-Terrestrial Environment, School of Space Science and Technology, Institute of Space Sciences, Shandong University, Weihai, China, [4]College of Science, Guilin University of Technology, Guilin, China, [5]Department of Earth and Space Sciences, Southern University of Science and Technology, Shenzhen, China

Abstract China's Chang'e-6 (CE-6) mission has returned the first-ever lunar farside samples from a mare plain on the southern Apollo basin floor. The crater statistics of the CE-6 mare unit and the provenance of the samples are crucial in interpreting the CE-6 sample analysis results and re-calibrating the crater chronology function. Here, we conduct a thorough survey of the formation sequence and main source craters of ejecta materials at the sampling area. Our results show that the sampling mare unit has a model age of ~2.8 Ga and the CE-6 scooped and drilled samples mainly come from the proximal ejecta of nearby small craters and the local regolith. The total abundance of foreign (non-mare) materials, primarily from Chaffee S and Vavilov craters, is ~9.3%. The Chaffee S ejecta may contain lunar upper mantle materials previously excavated by the South Pole-Aitken impact, which will shed light on the materials of the Moon's interior.

Plain Language Summary In June 2024, China's Chang'e-6 probe successfully returned the first-ever lunar farside samples of 1,935.3 g, from the Apollo basin within the South Pole Aitken (SPA) basin, the largest, deepest, and oldest impact basin on the Moon. The age and sources of the samples are vital in understanding the geological history of the landing region and the whole Moon. In this study, we obtain the model ages of the Chang'e-6 mare unit by impact crater statistics and conduct a thorough survey of the foreign ejecta materials from nearby and distal crater ejecta. We find that the Chang'e-6 scooped and drilled samples are mainly from the proximal ejecta of nearby small craters and the local regolith, both having a dominant composition of intermediate-Ti mare basalts. The surface age of the Chang'e-6 mare unit is ~2.8 billion years from crater density measurements, which can facilitate the refinement of lunar chronology function. Foreign (non-mare) materials likely account for a minor fraction (~9.3%) of the returned samples, primarily from Chaffee S and Vavilov craters. The Eratosthenian-aged Chaffee S crater may have delivered lunar upper mantle materials previously excavated by the SPA impact, which could potentially be recognized in the Chang'e-6 samples.

Key Points:

- The Chang'e-6 scooped samples are predominantly from local ejecta, and the drilled samples mostly originate from local ejecta and regolith
- Both samples are mainly composed of local basalts, with a model age of ~2.8 Ga, and foreign materials make up a minor fraction (~9.3%)
- Chaffee S crater delivered the most foreign materials, which may contain deep-seated materials and be collected by the Chang'e-6 mission

Supporting Information:

Supporting Information may be found in the online version of this article.

Correspondence to:

L. Xu and L. Qiao,
lyxu@must.edu.mo;
leqiao@sdu.edu.cn

Citation:

Xu, L., Qiao, L., Xie, M., Wang, Y., Zhu, M.-H., & Yan, J. (2024). Chronology, local stratigraphy, and foreign ejecta materials at the Chang'e-6 landing site: Constraints on the provenance of samples returned from the Moon's farside. *Geophysical Research Letters*, *51*, e2024GL111311. https://doi.org/10.1029/2024GL111311

Received 10 JUL 2024
Accepted 15 NOV 2024

Author Contributions:

Conceptualization: Luyuan Xu
Data curation: Luyuan Xu
Formal analysis: Luyuan Xu
Funding acquisition: Luyuan Xu, Le Qiao
Investigation: Luyuan Xu
Methodology: Luyuan Xu, Le Qiao, Minggang Xie
Project administration: Luyuan Xu
Validation: Luyuan Xu
Visualization: Luyuan Xu, Yiran Wang
Writing – original draft: Luyuan Xu, Le Qiao, Minggang Xie

© 2024. The Author(s).
This is an open access article under the terms of the Creative Commons Attribution-NonCommercial-NoDerivs License, which permits use and distribution in any medium, provided the original work is properly cited, the use is non-commercial and no modifications or adaptations are made.

1. Introduction

Extraterrestrial samples record precious information about the formation and evolution of the planetary bodies and the solar system (e.g., Spohn et al., 2014). So far, the Moon is the only terrestrial large body which has been sampled by crewed or robotic space missions. However, due to many technical challenges, all the returned lunar samples were collected from the nearside of the Moon by the United States' Apollo, Soviet's Luna, and China's Chang'e missions, and the lunar farside remains unsampled until 2024.

In June 2024, China's Chang'e-6 (CE-6) probe successfully landed on the southern floor of the Apollo basin (Figure 1a) and returned the first-ever lunar farside samples of 1,935.3 g (Li et al., 2024) by scooping (a few centimeters deep) and drilling (up to 2 meters deep; Zhou et al., 2022). Apollo basin is a large peak-ring impact basin (~510 km diameter) located at the inner edge of the South Pole-Aitken (SPA) basin (over 2,000 km diameter), the largest and oldest impact structure preserved on the Moon (Garrick-Bethell & Miljković, 2018; Garrick-Bethell & Zuber, 2009). The landing site of CE-6 mission (153.9856°W, 41.6383°S; Liu et al., 2024,

Writing – review & editing: Luyuan Xu, Le Qiao, Minggang Xie, Yiran Wang, Meng-Hua Zhu, Jianguo Yan

Figure 1a) is located on a mare basalt unit of a high-Fe (17–20 wt.%) and intermediate-Ti (3–6 wt.%) composition (Figure 1b; e.g., Jia et al., 2024; Qian, Head, Michalski, Wang, et al., 2024), within the Mg-pyroxene annulus dominated by abundant Mg-rich pyroxenes (Moriarty & Pieters, 2018). This mare unit was provisionally named Region F before the CE-6 landing (Zeng et al., 2023) and is termed as "Chang'e-6 mare unit" in this study.

Analyses of the Chang'e-6 samples collected from such a unique location provide an extraordinary opportunity to assess a number of fundamental questions concerning the origin and evolution of the Moon. First, the Chang'e-6 landed directly on a mare plain on the southern Apollo basin floor. Detailed laboratory high-accuracy analyses of the Chang'e-6 basaltic samples will provide crucial insights into the volcanism on the lunar farside, especially why volcanic mare deposits are much less areally abundant on the farside than those on the nearside? Are the nearside and farside basalts obviously different in the composition or depth of the source magma? Second, previous crater population analyses of the basaltic deposits surrounding the Chang'e-6 landing site reported surface model ages around 2.4–3.0 Ga (e.g., Qian, Head, Michalski, Wang, et al., 2024; Yue et al., 2024; Zeng et al., 2023), which lies in the age gap of the existing returned lunar samples. Precise age determination of the Chang'e-6 mare basalts by radio-isotopic analysis and crater statistics will be critically important for re-calibrating the lunar cratering chronology function (CF), the cornerstone for dating planetary surfaces in the inner solar system. Finally, the SPA basin-forming impact should have excavated and exposed deep lunar materials from the lower crust and even the upper mantle (e.g., Citron et al., 2024; Melosh et al., 2017; Potter et al., 2018). Those SPA-related materials could have been excavated and re-distributed through Apollo and subsequent impacts (e.g., Melosh et al., 2017; Moriarty et al., 2021; Orgel et al., 2024), potentially reaching the Chang'e-6 landing site and contributing foreign (non-mare) materials to the returned samples. In summary, accurate analyses of the age, composition, and provenance of the Chang'e-6 samples will potentially provide key evidence for constraining the geological history and interior nature of the Moon.

In this work, to assist the Chang'e-6 sample analyses, we carefully measure the crater density on surface units surrounding the CE-6 landing site, examine all possible main sources of foreign materials by ejecta ballistic sedimentation models, and quantitatively evaluate their contributions to the local stratigraphy and composition. Based on those investigations, we also discuss the scientific potential of the Chang'e-6 samples in revealing the lunar interior and recalibration of the lunar chronology function.

2. Method: Age Determination and Ejecta Thickness Estimation

We estimate the absolute model ages (AMAs) of the CE-6 mare unit and potential key ejecta source craters, from crater density and rock abundance, and distinguish whether an ejecta source crater forms after or before the Chang'e-6 mare unit through their relative ages or cross-cutting relationships (see Text S1–S3 and Table S1 in Supporting Information S1 for details of image data and age determination). We evaluate the ejecta thickness at the Chang'e-6 landing site from all lunar craters ≥10 km in diameter from the Robbins (2019) crater catalog, the median-sized craters ($D \geq 1$ km) surrounding the Apollo basin region identified by Ivanov et al. (2018), and the small craters ($D > 10$ m) identified in the vicinity of the landing site. The ages of key small craters are estimated from their degradation states (see Text S2 and Figure S1 in Supporting Information S1 for details).

For most craters/basins studied in this work, the ejecta thickness model of Pike (1974), which is widely accepted and most consistent with the Yutu-2 Lunar Penetrating Radar (LPR) investigations (see Xu et al. (2021) for the comparison of several ejecta thickness models), is applied to estimate the primary ejecta thickness (δ) from a given source crater/basin to the CE-6 landing site:

$$\delta = 0.033 R_t (r/R_t)^{-3.0} \quad (1)$$

where r is the spherical distance from the crater/basin center to the landing site and R_t is the transient rim-to-rim radius of the crater/basin. According to Melosh (1989) and Xie, Liu, and Xu (2020), we consider $R_t = 0.84$ R for simple craters and $R_t = 0.84 R_{SC}^{0.15} R^{0.85}$ for complex craters, where R is the final rim-to-rim radius measured from images, $R_{SC} = 9.5$ km is the transition radius from simple to complex craters (Pike, 1980). For large basins with dedicated investigations of impact cratering process and ejecta thickness distributions, the transient rim diameters of Orientale, Schrödinger, and Imbrium are referred to the studies of Xie and Zhu (2016), Xu and Xie (2020), and Miljković et al. (2013), and the primary ejecta thickness of Orientale and Schrödinger basin are computed from individual measurements of Xie and Zhu (2016) and Xu and Xie (2020), respectively. In addition, the distance and

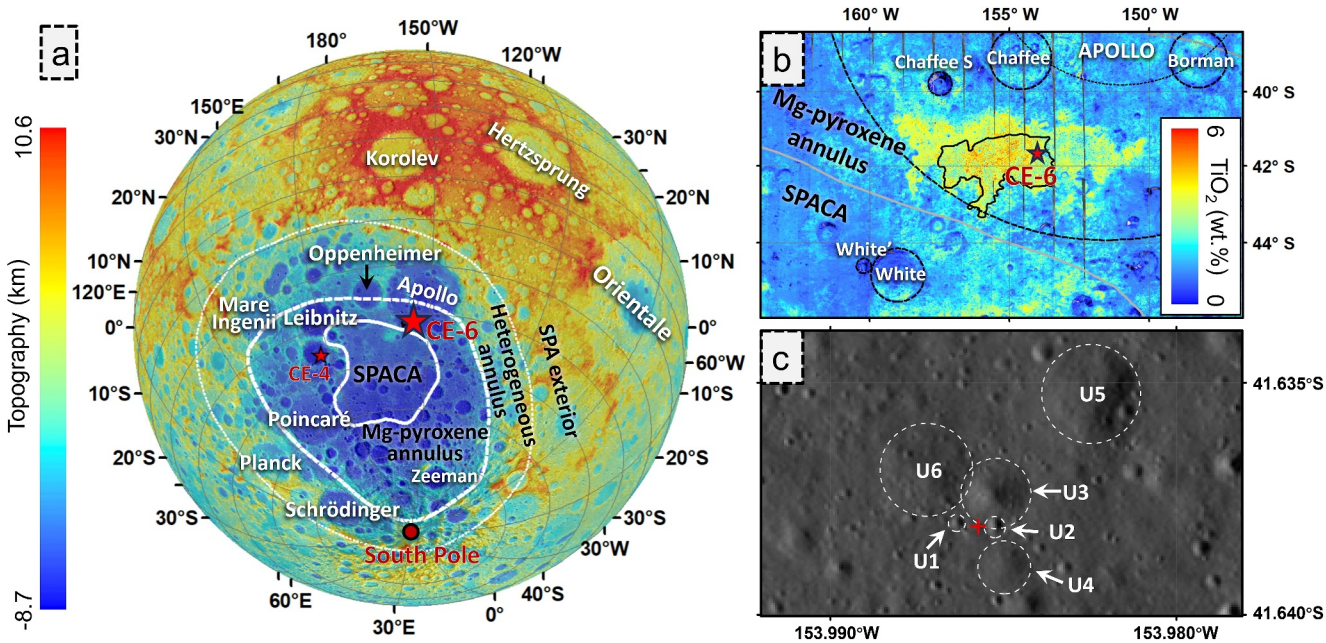


Figure 1. Geologic context surrounding the Chang'e-6 (CE-6) landing site. (a) Location of the Apollo basin and the CE-6 landing site. Lunar Orbiter Laser Altimeter (LOLA) topography and orthographic projection centered at the CE-6 landing site. Four concentric zones across the South Pole-Aitken (South Pole Aitken (SPA)) basin with different pyroxene compositions, including the SPACA (the central compositional anomaly of SPA), Mg-pyroxene annulus, heterogeneous annulus, and SPA exterior, are outlined according to Moriarty & Pieters (2018). (b) Kaguya Multiband Imager TiO_2 abundance map (~60 m/pixel; Yang et al., 2023) surrounding the CE-6 mare unit (delineated by the black curves). (c) Key local craters (labeled as U1–U6) surrounding the CE-6 landing site (marked by the red cross). U is short for "unnamed" crater. Lunar Reconnaissance Orbiter Narrow Angle Camera (LROC NAC) images (M1305784636 R, 1.88 m/pixel resolution, 78.94° incidence angle). All maps of the local Chang'e-6 landing area are projected into Mercator projection, unless otherwise specified.

deposition corrections are employed with the consideration of the curvature of the Moon (see Xu et al. (2021) for details). These corrections are vital for distal craters at a distance >1,500 km. In this work, we assume that the ejecta are symmetrically distributed surrounding the parent crater/basin, so the estimated ejecta thickness is mainly of statistical significance, as the actual ejecta distribution is probably rather inhomogeneous.

The depths of local materials mixed with foreign ejecta materials are estimated by Oberbeck et al. (1975) and the modified relationship of Petro and Pieters (2004, 2006, 2008), from a ratio (μ') of the thickness of the local materials to the primary ejecta:

$$\mu' = \begin{cases} \mu, & \mu \ll 5 \\ \mu/2 + 2.5, & \mu > 5 \end{cases} \quad (2)$$

where $\mu = 0.0183r^{0.87}$ and r is in the unit of km. The ejecta deposits are defined as the mixture of primary ejecta and local materials.

3. Results and Analyses

3.1. Crater Measurements and Ages of the Mare Basalts at the Chang'e-6 Landing Site

A characteristic kink is observed at ~1.0–1.2 km diameter in the cumulative size-frequency distribution (CSFD) plot of the measured impact craters superposed on the Chang'e-6 mare unit (Figure S2 in Supporting Information S1), indicating the occurrence of volcanic resurfacing, and the last phase of lava flows did not completely bury all the pre-existing craters. In addition, we also find several pre-existing craters, which were partially buried (Figure S3 in Supporting Information S1) or abnormally shallow (Figure S4; see Text S2 and S3 in Supporting Information S1 for details), on the Chang'e-6 mare unit, consistent with the interpretation of at least two-phased volcanic eruptions of Qian, Head, Michalski, Wang, et al. (2024). Spectral investigation of penetrating craters showed the underlying basalts have considerably lower TiO_2 abundance than the upper basalt layer (Qian, Head,

Michalski, Wang, et al., 2024). From the CSFD plot deflection occurrence diameter, the uppermost thickness at the thinnest region of the upper basalt layer can be estimated as ~50–60 m (Haruyama et al., 2009; Pike, 1977), in line with estimations from crater excavation technique (Qian, Head, Michalski, Wang, et al., 2024).

By carefully excluding those pre-existing craters (see Text S3 in Supporting Information S1 for details), an $N(1)$ value of 2.16 ($\pm$0.09) $\times$ 10^{-3} km^{-2} are obtained by using Kaguya Terrain Camera Morning images (10 m/pixel; Haruyama et al., 2008) and fitting craters $D \geq 300$ m, which projects to a formation age of $2.80^{+0.10}_{-0.11}$ Ga for the upper basalt layer (Figure 2b and Table S2 in Supporting Information S1). The crater statistics within a 5 km diameter circle across the landing site using Lunar Reconnaissance Orbiter Narrow Angle Camera (LROC NAC) images (~1 m/pixel; Robinson et al., 2010) also yield a very close age of $2.79^{+0.34}_{-0.51}$ Ga (Figure S5 and Table S2 in Supporting Information S1). Since the relatively smaller crater population working area and an equilibrium onset diameter around ~150 m (Figure S5b in Supporting Information S1), we can only fit the relatively larger ($D \geq 160$ m), but fewer craters in the LROC NAC crater population investigation, which inevitably results in a much higher uncertainty in the age determination. Still, the close age from LROC NAC image counts validates our crater measurements and age determination for the CE-6 upper basalts layer. We also compare our results with previous studies (Figure 2c, Text S4, and Table S3 in Supporting Information S1) and find they are generally consistent with each other.

Then, we turn to the larger diameter (>1.2 km) segment of the CSFD curve and fit a $N(1)$ value of 6.63 ($\pm$2.19) $\times$ 10^{-3} km^{-2} and AMA of $3.60^{+0.07}_{-0.12}$ Ga (Figure 2b and Table S2 in Supporting Information S1). Given that the upper basalt layer varies in thickness (Qian, Head, Michalski, Wang, et al., 2024), we suggest that a part of the pre-existing craters larger than 1.2 km probably have been totally buried, and therefore, the estimated ~3.6 Ga can be interpreted as the lower limit of the formation age of the underlying basalt layer.

In summary, our crater statistics results show that the overlaying intermediate-Ti basalts of the CE-6 landing site erupted at ~2.8 Ga of Eratosthenian period, and the underlying low-Ti basalts emplaced at no earlier than ~3.6 Ga of Late Imbrian period. We term these two basalt layers as "CE-6 Eratosthenian mare unit" and "CE-6 Imbrian mare unit" hereafter.

3.2. Ages of Key Source Craters Related to the Stratigraphy at the Chang'e-6 Landing Site

Based on the ejecta thickness computation, several potential source craters are identified (Table 1). Among them, the modeled ages of four key ones are determined through crater counts: White' (805^{+50}_{-50} Ma), Vavilov ($1.86^{+0.12}_{-0.12}$ Ga), Chaffee S ($2.79^{+0.23}_{-0.28}$ Ga), and White ($3.48^{+0.04}_{-0.06}$ Ga), with their CSFD plots and fitted $N(1)$ values shown in Figure S6 and Table S2 in Supporting Information S1, respectively. Ages of the other seven key source craters with reported $N(1)$ values or rock abundance ages from literature are re-derived based on the chronology function of Yue et al. (2022): Crookes (488 Ma), Das (719 Ma), Pythagoras ($2.34^{+0.17}_{-0.17}$ Ga), Antoniadi ($3.47^{+0.02}_{-0.02}$ Ga), Hausen ($3.66^{+0.02}_{-0.03}$ Ga), Dryden ($3.68^{+0.03}_{-0.03}$ Ga), and Maksutov ($3.71^{+0.03}_{-0.03}$ Ga) (See Text S1 and Table S4 in Supporting Information S1 for details). In addition, the ages of nine top local ejecta source craters in the vicinity of the CE-6 landing site, ranging from ~0.4 Ma to ~140 Ma, are estimated by their degradation states (See Text S2 in Supporting Information S1 for details). The locations of those craters are shown in Figure S7, S8 in Supporting Information S1, and Figure 1c.

3.3. Ejecta Thickness of Major Post- and Pre-Mare Craters at the Chang'e-6 Landing Site

Three Copernican craters delivered primary ejecta thicker than 0.35 cm to the CE-6 landing site: Crookes (0.37 cm), Das (0.49 cm), and White' (0.41 cm), and three Eratosthenian-aged craters delivered primary ejecta thicker than 0.35 cm: Vavilov (1.72 cm), Pythagoras (0.64 cm), and Chaffee S (15.61 cm) (from the youngest to the oldest; Table 1 and Figure S7 in Supporting Information S1). The former five craters are significantly younger than CE-6 Eratosthenian mare unit ($2.80^{+0.10}_{-0.11}$ Ga) based on their modeled ages, and although Chaffee S crater ($2.79^{+0.23}_{-0.28}$ Ga) has a very close modeled age, the extensive rays observed on the CE-6 Eratosthenian mare unit (Figure 2a; Orgel et al., 2024) undoubtedly show that Chaffee S crater is younger. Therefore, all the six craters emplaced ejecta overlaying on the CE-6 Eratosthenian mare unit. Among them, the Eratosthenian-aged Chaffee S crater delivered the most foreign materials and is the only decimeter-level ejecta contributor to the CE-6 Eratosthenian mare unit. No Eratosthenian craters identified by Ivanov et al. (2018), except for Chaffee S, can contribute nonnegligible ejecta on the CE-6 Eratosthenian mare unit (See Text S5 and Table S5 in Supporting

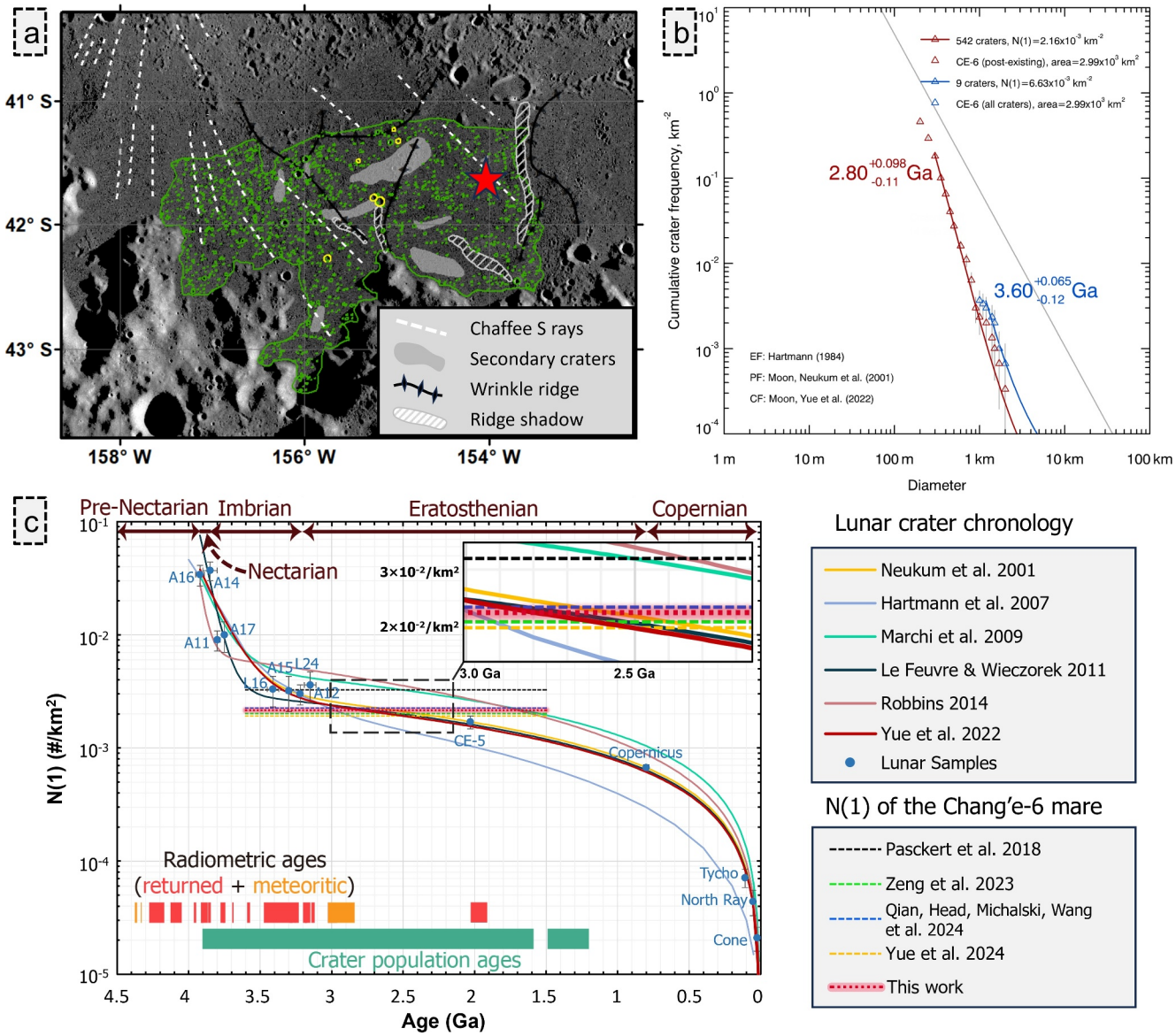


Figure 2. Crater population measurements for the Chang'e-6 (CE-6) mare unit. (a) Spatial distribution of craters ≥200 m in diameter (post- and pre-existing craters shown by green and yellow circles, respectively) within the CE-6 mare unit (outlined by the green curve; Zeng et al., 2023), with the CE-6 landing site marked by the red star. Kaguya Terrain Camera Morning mosaic. The spatial distribution of Chaffee S rays (white dashed lines) is from Orgel et al. (2024). (b) The cumulative size-frequency distribution (CSFD) plot of the post-existing craters ($D \geq 200$ m) and all craters ($D \geq 1$ km) within the CE-6 mare unit. The gray line shows the lunar equilibrium function (EF) from Hartmann (1984), and the production function (PF) of Neukum et al. (2001) and the chronology function (CF) of Yue et al. (2022) are employed. (c) $N(1)$ values and their corresponding modeled ages of the CE-6 Eratosthenian mare unit, derived from lunar chronology functions of Neukum et al. (2001), Hartmann et al. (2007), Marchi et al. (2009), Le Feuvre and Wieczorek (2011), Robbins (2014), and Yue et al. (2022), as shown by the various colored solid curves, respectively. Figure updated from Qiao et al. (2021). The $N(1)$ values reported in this study (red) and previous works (other colors) are plotted as horizontal dotted lines, respectively. For the data of calibration points, including Apollo (A), Luna (L), Chang'e (CE), and lunar samples from other known locations, radio-isotopic ages are from Stöffler and Ryder (2001) and Li et al. (2021), and $N(1)$ values are from Neukum (1983), Hiesinger et al. (2012), Robbins (2014), and Qiao et al. (2021). Radio-isotopic ages range of returned and meteoritic lunar basalts (from Tartèse et al. (2019), Li et al. (2021), and Che et al. (2021)) and absolute model ages (AMAs) by crater statistic of lunar mare units (Qiao et al., 2020) are shown at the bottom. Lunar chronostratigraphic system is shown at the top according to Stöffler and Ryder (2001).

Information S1 for details). We also investigate nine top local source craters (U1-U9 in Table 1 and Figure S8 in Supporting Information S1) around the CE-6 landing site and find that a 46 m-sized crater U3 (~8 Ma) contributed the most local ejecta (~20 cm thick) to the landing site. The total thickness of those local ejecta deposits is ~0.3 m.

Table 1
Ages, Formation Sequence, and Ejecta Thickness of Main Contributing Basins/Crater to the CE-6 Landing Site

	Source crater/basin	Final diameter (km)[a]	Longitude (°)[a]	Latitude (°)[a]	Spherical distance (km)	Periods (Losiak et al., 2009)[b]	Absolute model ages (AMAs)[c]		Primary ejecta (m)	Local materials (m)	Ejecta deposits (m)
local ejecta	U1[d]	0.011	−153.986	−41.638	0.014	–	0.4 Ma	**Copernican**	0.005	0.0000	0.005
	U2	0.014	−153.985	−41.638	0.011	–	1.9 Ma		0.020	0.0000	0.020
	U3	0.046	−153.985	−41.637	0.024	–	8.4 Ma		0.201	0.0001	0.201
	U4	0.035	−153.985	−41.639	0.032	–	10 Ma		0.023	0.0000	0.023
	U5	0.065	−153.982	−41.635	0.114	–	21 Ma		0.006	0.0000	0.006
	U6	0.061	−153.987	−41.637	0.050	–	33 Ma		0.034	0.0000	0.034
	U7	0.132	−153.982	−41.630	0.252	–	99 Ma		0.004	0.0000	0.004
	U8	0.198	−153.995	−41.624	0.462	–	137 Ma		0.004	0.0000	0.004
	U9	0.165	−153.982	−41.644	0.193	–	143 Ma		0.021	0.0001	0.021
foreign ejecta	Crookes	49.2	−165.10	−10.39	992.8	Cc	488 Ma[e]	**Copernican**	0.004	0.023	0.027
	Das	35.8	−137.06	−26.50	623.2	Cc	719 Ma[e]		0.005	0.024	0.029
	White'[f]	11.5	−160.21	−44.59	164.2	–	805^{+50}_{-50} Ma		0.004	0.006	0.010
	Vavilov	96.4	−138.77	−0.89	1,303.8	Cc	$1.86^{+0.12}_{-0.12}$ Ga	**Eratosthenian**	0.017	0.123	0.141
	Pythagoras	127.6	−63.02	63.58	3,848.5	Ec	$2.34^{+0.17}_{-0.17}$ Ga[g]		0.006	0.092	0.099
	Chaffee S[h]	19.6	−157.49	−39.77	98.4	–	$2.79^{+0.23}_{-0.28}$ Ga		0.156	0.155	0.311
	CE-6 Eratosthenian mare unit						**$2.80^{+0.10}_{-0.11}$ Ga**		–	–	–
	Antoniadi	137.9	−172.99	−69.40	893.7	Ic2	$3.47^{+0.02}_{-0.02}$ Ga[i]	**Late Imbrian**	0.17	0.98	1.14
	White	41.1	−159.00	−44.82	146.8	Ic2	$3.48^{+0.04}_{-0.06}$ Ga		0.58	0.81	1.39
	CE-6 Imbrian mare unit						**$>3.60^{+0.07}_{-0.12}$ Ga**		–	–	–
	Hausen	165.0	−88.57	−65.20	1,298.3	Ec	$3.66^{+0.02}_{-0.03}$ Ga[j]		0.11	0.77	0.88
	Dryden	54.5	−156.17	−33.21	260.9	Ic2	$3.68^{+0.03}_{-0.03}$ Ga[k]		0.27	0.63	0.90
	Maksutov	84.5	−168.64	−40.79	335.0	Ic2	$3.71^{+0.03}_{-0.03}$ Ga[k]		0.57	1.63	2.20
	Orientale (the youngest)	941.0	−95.24	−19.83	1,632.3	Ic1	–	**Early Imbrian**	28.95	237.69	266.64
	Schrödinger	321.5	133.06	−74.77	1,385.3	Ic1	–		1.16	8.66	9.82
	Imbrium (the oldest)	1,198.4	−17.14	34.26	4,413.5	Ic1	–		9.36	150.35	159.71
	Crisium	1,114.5	59.46	16.40	4,299.6	Nc	–	**Nectarian (unknown order)**	10.55	166.33	176.89
	Oppenheimer	202.3	−166.02	−35.35	343.0	Nc	–		10.16	29.86	40.02
	Serenitatis	866.2	22.86	27.02	5,008.1	Nc	–		10.03	177.00	187.03
	Chaffee	51.9	−154.60	−39.08	79.0	Nc	–		8.23	6.74	14.97
	Chawla'[l]	92.7	−147.12	−42.64	157.3	–	–		7.46	11.13	18.60
	Hertzsprung	558.8	−129.38	1.96	1,485.2	Nc	–		4.55	35.28	39.83
	Korolev	429.7	−157.47	−4.38	1,133.6	Nc	–		3.92	26.09	30.01

Table 1
Continued

Source crater/ basin	Final diameter (km)[a]	Longitude (°)[a]	Latitude (°)[a]	Spherical distance (km)	Periods (Losiak et al., 2009)[b]	Absolute model ages (AMAs)[c]	Primary ejecta (m)	Local materials (m)	Ejecta deposits (m)
Humorum	796.4	−39.40	−25.96	2,709.5	Nc	–	3.88	44.14	48.02
Nectaris (the oldest)	872.0	34.76	−15.83	3,698.4	Nc	–	3.99	56.40	60.39

[a]The final diameters, longitudes, and latitudes of craters ($D \geq 10$ km) are according to the crater database of Robbins (2019). [b]Cc, Ec, Ic2, Ic1, and Nc are short for Copernican, Eratosthenian, Late Imbrian, Early Imbrian, and Nectarian craters, respectively. [c]All AMAs are derived from the CF of Yue et al. (2022). $N(1)$ values see Table S2 and S3 in Supporting Information S1. Locations of those craters are shown in Figure S7, S8 in Supporting Information S1, and Figure 1c. We emphasize that the relative formation order of those ejecta source craters and the mare basalts, rather than the derived absolute ages (or the $N(1)$ values), is more important for determining the stratigraphy. The model ages of the mare units are in bold. [d]U is short for "unnamed" crater, and the thickness of local ejecta are derived from those source craters' initial diameters before degradation (Figure S1 in Supporting Information S1). [e]Age converted from rock abundance of Mazrouei et al. (2019). [f]Identified as Eratosthenian crater (Ec) in Ivanov et al. (2018). [g]Age converted from crater counts of Hou et al. (2022). [h]Identified as Copernican crater (Cc) in Ivanov et al. (2018) and Orgel et al. (2024). [i]Age converted from crater counts of Krasilnikov et al. (2023). [j]Age converted from crater counts of Xie, Xiao, et al. (2020). [k]Age converted from crater counts of Ivanov et al. (2018). [l]Geological age refers to Fortezzo et al. (2020).

Five Late Imbrian-aged craters transported primary ejecta thicker than 10 cm to the CE-6 landing site: Antoniadi, White, Hausen, Dryden, and Maksutov (from the youngest to the oldest; Table 1 and Figure S7 in Supporting Information S1). Among them, Antoniadi (16.6 cm) and White (57.8 cm) may form between the two eruptions of the CE-6 Eratosthenian and Imbrian mare units, based on the crater dating results. Although White crater is identified as an Eratosthenian-aged crater in the geologic map of Fortezzo et al. (2020), no ejecta or secondary craters on the CE-6 Eratosthenian mare unit can be traced back to this crater, suggesting that White crater is at least older than the CE-6 Eratosthenian mare unit, which agrees well with our dating result ($3.48^{+0.04}_{-0.06}$ Ga). Those two source craters delivered a total primary ejecta of 0.74 m and may form ejecta deposits of 1.56 m thick between the two mare units at the CE-6 landing site. The other three craters, Hausen (10.7 cm), Dryden (27.1 cm), and Maksutov (56.8 cm), are possibly pre-dated the eruption of the CE-6 Imbrian mare unit, and thus emplaced ejecta under this unit. In total, those three craters delivered primary ejecta of 0.95 m and created ejecta deposits of 2.58 m thick.

Three Early Imbrian basins delivered primary ejecta thicker than 1 m: Orientale (29.0 m), Schrödinger (1.2 m), and Imbrium (9.4 m) (from the youngest to the oldest; Table 1 and Figure S7 in Supporting Information S1). Below those ejecta, nine Nectarian craters/basins delivered primary ejecta thicker than 2 m, with the most dominant four are Crisium (10.6 m), Oppenheimer (10.2 m), Serenitatis (10.0 m), and Chaffee (8.2 m). However, since the relative age of those Nectarian craters/basins are uncertain, the detailed emplacement sequence and the ejecta deposits thickness cannot be determined. In summary, all the Early Imbrian and Nectarian craters/basins listed in Table 1 delivered primary ejecta of 39.5 and 62.8 m and created ejecta deposits of 266.6 m and > ~200 m, respectively, below the CE-6 Imbrian mare unit.

4. Discussion

4.1. The Geological History, Emplacement Sequence of Principal Ejecta, and a Possible Geological Stratigraphy at the Chang'e-6 Landing Site

Both our crater statistic results and previous studies (e.g., Qian, Head, Michalski, Wang, et al., 2024; Zeng et al., 2023) show that the CE-6 sampling region has experienced a complex geological history after the formation of the SPA basin. The proposed formation sequence is shown in Table 1 and Figure 3.

As the deepest probe to the lunar interior, SPA impact possibly excavated the upper mantle materials and delivered ejecta, as well as impact melts and breccias over tens of kilometers in thickness (e.g., Citron et al., 2024; Melosh et al., 2017; Potter et al., 2018), to the region beneath the CE-6 landing site. Subsequently, those deep-originated materials can be re-excavated and transported to the landing site by the Apollo basin, which formed on the proximal ejecta blankets of the SPA basin (Moriarty et al., 2021; Orgel et al., 2024). After that, several Nectarian basins/craters delivered ejecta above. Those Nectarian ejecta deposits are estimated to be thicker than

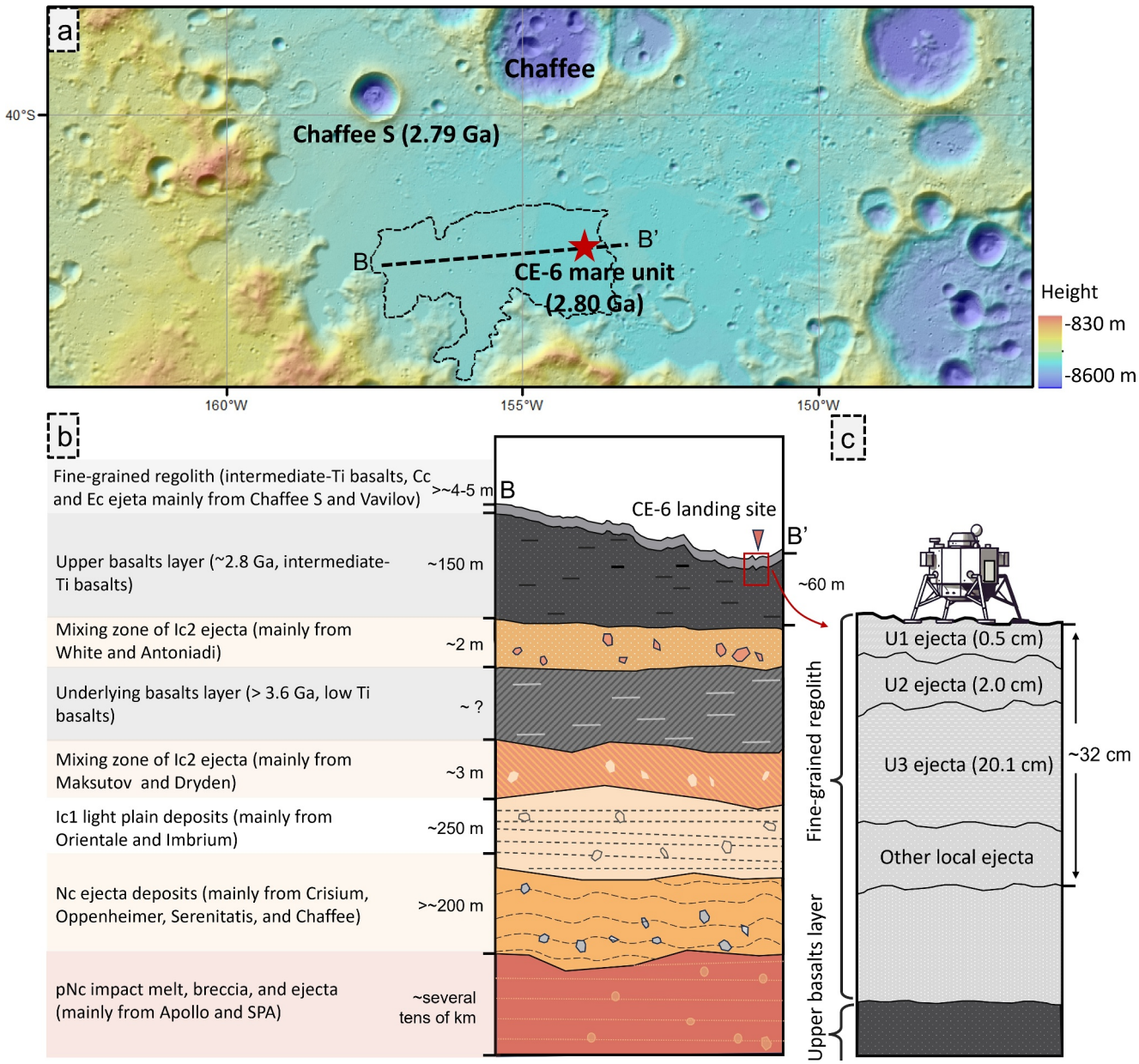


Figure 3. Proposed geological stratigraphy beneath the Chang'e-6 landing region. (a) Topography surrounding the CE-6 landing region, with the landing site marked by the red star. SELENE/Kaguya TC + Lunar Reconnaissance Orbiter (LRO) Lunar Orbiter Laser Altimeter (LOLA) merged Digital Elevation Model (SLDEM2015; 512 pixels/degree; Barker et al., 2016) overlaying on its shaded relief. (b) Geological stratigraphy at the Chang'e-6 landing region, with the shallow stratigraphy within the regolith layer shown in panel (c). The surface topographic profile in panel (b) is extracted from SLDEM along BB' shown in panel (a). The decreasing thicknesses of the CE-6 Imbrian mare basalt layer from the west to the east in panel (b) are referred to Qian, Head, Michalski, Wang, et al. (2024). Thicknesses of those layers are not to scale. Note that these stratigraphic illustrations are mainly used to represent the formation sequence and overlapping relationships of these ejecta layers. Some layers may have undergone significant mixing, resulting in the destruction of the original interfaces.

~200 m, mainly from Crisium, Oppenheimer, Serenitatis, and Chaffee. Overlaying on the Nectarian ejecta layer, light plains deposits of ~250 m in thickness, mainly composed of Early Imbrian-aged Orientale and Imbrium ejecta, are expected to deposit here. The voluminous ejecta from Orientale basin are indicated by multiple large secondary craters (Guo et al., 2018) and the light plains deposits observed near the CE-6 mare unit (Meyer et al., 2020).

Shortly following this, a thin mixing layer (~3 m) of Late Imbrian ejecta piled up at ~3.7 Ga, mainly from Maksutov and Dryden craters. Then, a volcanic eruption occurred at ~3.6 Ga, emplacing the low-Ti basalts (i.e., the CE-6 Imbrian mare unit). This mare unit was subsequently buried by another thin mixing layer (~2 m) of Late Imbrian ejecta, mainly from White and Antoniadi craters. Alternatively, since ~3.6 Ga is a lower limit age of the CE-6 Imbrian mare unit, this volcanic eruption possibly occurred earlier and was covered by those two thin layers of Late Imbrian ejecta.

At ~2.8 Ga, another volcanic eruption occurred and emplaced the intermediate-Ti basalts (i.e., the CE-6 Eratosthenian mare unit) on the pre-existing stratigraphy, with thicknesses decreasing from ~150 m in the east to ~60 m in the west (Qian, Head, Michalski, Wang, et al., 2024). After that, the ejecta from Eratosthenian and Copernican-aged craters deposited, creating an ejecta deposits layer of ~34 cm thick above. In parallel, impact bombardments continuously pulverized and mixed the topmost layers at the CE-6 landing site, producing a loose, fine-grained regolith layer (Melosh, 1989). Since the thickness of regolith statistically increases with the surface age (Melosh, 1989; Xie et al., 2021), we estimate the median regolith thickness at the CE-6 landing site to be larger than that at the CE-5 landing site (~2.0 Ga; Li et al., 2021; Che et al., 2021), which is ~4–6 m (Qian et al., 2021). In addition, Orgel et al. (2024) reported an average regolith thickness of 4.6 m for a mare region close to the CE-6 landing site, agreeing well with this estimation. In summary, we consider that the median thickness of the regolith layer at the CE-6 landing site is at least ~4–5 m. As this regolith layer is considerably thicker than the combined Eratosthenian and Copernican ejecta deposits, all these ejecta, along with a part of the underlying intermediate-Ti basalts, were mixed into the regolith layer. Finally, small young craters near the landing site generated a local ejecta of ~32 cm thick and overturned the regolith at the landing site.

4.2. The Provenance of the Foreign Materials in the Chang'e-6 Samples

Based on the ejecta thickness estimations and the relative ages of source craters, the top four foreign source craters delivering nonnegligible primary ejecta are: Chaffee S (15.6 cm), Vavilov (1.7 cm), Pythagoras (0.6 cm), and Das (0.5 cm). Those craters produced a total of 18.4 cm-thick primary ejecta on the CE-6 landing site. Using the analytic impact gardening model of Costello et al. (2020) and extending the timescale to 2.79 Ga, the overturn depth (with 99% probability of at least one overturn) at the CE-6 landing site is 2.08 m, resulting in a compositional percentage of foreign materials from Chaffee S of 7.5%. By applying a similar methodology, the abundances of foreign materials from craters Vavilov, Pythagoras, and Das are estimated to be 1.0%, 0.34%, and 0.46%, respectively.

The laboratory analyses of the CE-5 samples revealed that the percentage of foreign materials is at least less than half of what was predicted by ejecta ballistic sedimentation models (Yang et al., 2022; Zong et al., 2022), possibly indicating that the ejecta burial of the nearby local craters may largely dilute the abundance of foreign materials. However, since there is no such large local crater like Xu Guanqi, a 410 m-sized crater near the CE-5 landing site (Jia et al., 2022), in the vicinity of the CE-6 landing site, this dilution effect may be less significant for the CE-6 samples. Therefore, we predict that the CE-6 samples are primarily composed of the upper intermediate-Ti basalts, with minor foreign materials (~9.3% in total) delivered from craters outside the mare unit. The largest proportion of foreign materials come from the Eratosthenian-aged Chaffee S crater ($D = 19.6$ km; Figure 3a), which is located ~45 km (<2 radii) away from the rim of Chaffee crater ($D = 51.9$ km), a Nectarian crater situated exactly at the peak ring of the Apollo basin. Since the peak ring materials represent the deepest materials exposed in the impact basin (Cintala & Grieve, 1998), and the Apollo basin lies at the proximal ejecta blankets of the SPA basin, both the SPA ejecta and the even deeper crust materials were possibly exposed to the Apollo's peak ring (Moriarty et al., 2021; Orgel et al., 2024). Therefore, Chaffee crater possibly excavated and transported both the lunar upper mantle materials, which were carried by SPA ejecta, and relatively primitive lunar crust materials, which were excavated by Apollo impact, to the surrounding regions. As shown in Table S6 in Supporting Information S1, before the formation of Chaffee S crater, ~200 m-thick of Nectarian ejecta deposits, including ~20 m in thickness from Chaffee crater, have emplaced on the southern Apollo basin floor. The Chaffee S impact, with an excavation depth of ~1.23 km by adopting an excavation depth of 1/10 of a transient crater diameter (Melosh, 1989), probably excavated and delivered those lunar deep materials to the CE-6 landing site, which is also supported by recent

spectral studies of the Apollo basin (e.g., Guo et al., 2024; Qian, Head, Michalski, Gong, et al., 2024; Sun & Lucey, 2024).

According to the formation sequences of the proximal ejecta (Table 1 and Figure 3c), the topmost layers are the U1-U3 ejecta with a total thickness of ~0.23 m, and the total local ejecta layer is ~0.32 m thick. Therefore, almost all the scooped samples from a few centimeters deep ought to originate from the local ejecta of those nearby small craters, and the drilled samples from up to 2 m deep are mainly comprised of both local ejecta and regolith. Based on their excavation depths, most ejecta of the nine small craters originate in depth less than ~4–5 m, and hence the local ejecta ought to share similar composition (mainly composed of the overlaying intermediate-Ti basalts) to the regolith.

In addition, since the CE-6 Eratosthenian mare unit was penetrated by some post-formed craters (Qian, Head, Michalski, Wang, et al., 2024), those craters could excavate the underlying Imbrian mare unit and possibly the Late Imbrian ejecta (mainly from White crater) layer and bring these underlying materials to the surface. Therefore, intermediate-Ca,Fe pyroxene, a typical composition of central SPA compositional anomaly (SPACA), identified at the wall and central peak of White crater (Moriarty & Pieters, 2018), might also be sampled by the CE-6 mission. However, since those penetrating craters contributed very few primary ejecta with a total thickness of only 0.21 cm (Table S7 in Supporting Information S1), the percentage of underlying low-Ti basalts plus possible Whie ejecta is likely to be very minor (<~0.1%).

4.3. Implications for the Re-Calibration of Lunar Crater Chronology Function

Based on our crater counts, the Eratosthenian mare unit, which was sampled by the Chang'e-6 mission, was dated to be ~2.8 Ga using the conventional cratering chronology function. However, the same crater density value would project onto model ages ranging from ~1.6 to ~3.0 Ga under alternative chronology functions (Figure 2c). One major reason for these uncertainties is the very limited number of calibration points of all the existing chronology functions. The radio-isotopic age of the returned Chang'e-6 basaltic samples likely lies in the age gap of those existing chronology functions. Combining our superposed crater population measurements and the radio-isotopic age of the Chang'e-6 samples will provide one new and critical calibration point for the lunar chronology function.

In addition, the Chang'e-6 samples may also contain ejecta materials from the Chaffee S crater, which probably have excavated the SPA and Apollo basin materials (although their abundance is likely very low). If those basin materials are identified in the Chang'e-6 samples, their radio-isotopic ages would be vital for anchoring >~3.9 Ga segment of the lunar chronology function and the early impact flux in lunar history.

5. Conclusion

In this study, we conduct a thorough survey of the crater statistics and the main ejecta materials from near and distal craters related to the Chang'e-6 mare unit. We find that at least two phases of mare basalts have emplaced on the Chang'e-6 landing region, with model ages of ~2.8 Gyr for the upper intermediate-Ti mare basalts and >3.6 Gyr for the underlying low-Ti mare basalts. Those modeled ages are derived from the crater density measurements and will be further calibrated by the isotopic dating of the CE-6 samples. The CE-6 scooped samples mainly from the proximal ejecta of nearby small craters, and the drilled samples mostly come from the local ejecta and regolith, both types of samples having a major composition of the local Eratosthenian intermediate-Ti mare basalts. The total amounts of foreign (non-mare) materials make up a minor component (~9.3%), mainly from Chaffee S (~7.5%) and Vavilov (~1.0%) craters. The Eratosthenian-aged Chaffee S crater may deliver lunar upper mantle materials excavated by the SPA and subsequent craters, which are expected to be collected by the CE-6 mission. These results can facilitate the analysis of the CE-6 lunar samples and the refinement of lunar chronology function.

Data Availability Statement

LROC images are archived in M. Robinson (2009), Kaguya/SELENE data can be downloaded from SELENE Data Archive (https://darts.isas.jaxa.jp/app/pdap/selene/index.html.en), SLDEM2015 topography data are available in Neumann (2009), and the Kaguya TiO_2 maps are available in Zhang (2023). The crater measurement data of this study are available in a public repository, see Xu (2024).

Acknowledgments
We greatly appreciate two anonymous reviewers for their valuable comments that improved the quality of the manuscript. This work was supported by the National Natural Science Foundation of China (12303064, 42241107, 12173011, 42201424, 42241116), Science and Technology Development Fund of Macau (0012/2023/RIA1; 0064/2022/A2), Open Research Fund Program of LIESMARS, Wuhan University (Grant 22P02), and Young Scholars Program of Shandong University, Weihai (202207).

References

Barker, M. K., Mazarico, E., Neumann, G. A., Zuber, M. T., Haruyama, J., & Smith, D. E. (2016). A new lunar digital elevation model from the lunar orbiter laser altimeter and SELENE terrain camera. *Icarus*, *273*, 346–355. https://doi.org/10.1016/j.icarus.2015.07.039

Che, X., Nemchin, A., Liu, D., Long, T., Wang, C., Norman, M. D., et al. (2021). Age and composition of young basalts on the Moon, measured from samples returned by Chang'e-5. *Science*, *374*(6569), 887–890. https://doi.org/10.1126/science.abl7957

Cintala, M. J., & Grieve, R. A. F. (1998). Scaling impact melting and crater dimensions: Implications for the lunar cratering record. *Meteoritics & Planetary Sciences*, *33*(4), 889–912. https://doi.org/10.1111/j.1945-5100.1998.tb01695.x

Citron, R. I., Smith, D. E., Stewart, S. T., Hood, L. L., & Zuber, M. T. (2024). The South Pole-Aitken basin: Constraints on impact excavation, melt, and ejecta. *Geophysical Research Letters*, *51*(14), e2024GL110034. https://doi.org/10.1029/2024GL110034

Costello, E. S., Ghent, R. R., Hirabayashi, M., & Lucey, P. G. (2020). Impact gardening as a constraint on the age, source, and evolution of ice on Mercury and the Moon. *Journal of Geophysical Research: Planets*, *125*(3), e2019JE006172. https://doi.org/10.1029/2019JE006172

Fortezzo, C. M., Spudis, P. D., & Harrel, S. L. (2020). Release of the digital unified global geologic map of the Moon at 1: 5,000,000-Scale. In *51st annual lunar and planetary science conference* (Vol. 2326, p. 2760).

Garrick-Bethell, I., & Miljković, K. (2018). Age of the lunar south Pole-Aitken basin. *49th Lunar and planetary science conference*.

Garrick-Bethell, I., & Zuber, M. T. (2009). Elliptical structure of the lunar South Pole-Aitken basin. *Icarus*, *204*(2), 399–408. https://doi.org/10.1016/j.icarus.2009.05.032

Guo, D., Bao, Y., Liu, Y., Wu, X., Xu, Y., Yang, Y., et al. (2024). Geological investigation of the lunar Apollo basin: From surface composition to interior structure. *Earth and Planetary Science Letters*, *646*, 118986. https://doi.org/10.1016/j.epsl.2024.118986

Guo, D., Liu, J., Head III, J. W., & Kreslavsky, M. A. (2018). Lunar Orientale impact basin secondary craters: Spatial distribution, size-frequency distribution, and estimation of fragment size. *Journal of Geophysical Research: Planets*, *123*(6), 1344–1367. https://doi.org/10.1029/2017JE005446

Hartmann, W. K. (1984). Does crater "saturation equilibrium" occur in the solar system? *Icarus*, *60*(1), 56–74. https://doi.org/10.1016/0019-1035(84)90138-6

Hartmann, W. K., Quantin, C., & Mangold, N. (2007). Possible long-term decline in impact rates: 2. Lunar impact-melt data regarding impact history. *Icarus*, *186*(1), 11–23. https://doi.org/10.1016/j.icarus.2006.09.009

Haruyama, J., Matsunaga, T., Ohtake, M., Morota, T., Honda, C., Yokota, Y., & LISM Working Group. (2008). Global lunar-surface mapping experiment using the Lunar Imager/Spectrometer on SELENE. *Earth Planets and Space*, *60*(4), 243–255. https://doi.org/10.1186/BF03352788

Haruyama, J., Ohtake, M., Matsunaga, T., Morota, T., Honda, C., Yokota, Y., et al. (2009). Long-lived volcanism on the lunar farside revealed by SELENE Terrain Camera. *Science*, *323*(5916), 905–908. https://doi.org/10.1126/science.1163382

Hiesinger, H. V., Van Der Bogert, C. H., Pasckert, J. H., Funcke, L., Giacomini, L., Ostrach, L. R., & Robinson, M. S. (2012). How old are young lunar craters? *Journal of Geophysical Research*, *117*(E12). https://doi.org/10.1029/2011JE003935

Hou, X., Fu, X., Qiao, L., Li, B., Yin, C., Zhang, J., & Ling, Z. (2022). Absolute model ages of three craters in the vicinity of the Chang'E-5 landing site and their geologic implications. *Icarus*, *372*, 114730. https://doi.org/10.1016/j.icarus.2021.114730

Ivanov, M. A., Hiesinger, H., Van Der Bogert, C. H., Orgel, C., Pasckert, J. H., & Head, J. W. (2018). Geologic history of the northern portion of the South Pole-Aitken basin on the Moon. *Journal of Geophysical Research: Planets*, *123*(10), 2585–2612. https://doi.org/10.1029/2018JE005590

Jia, B., Fa, W., Zhang, M., Di, K., Xie, M., Tai, Y., & Li, Y. (2022). On the provenance of the Chang'E-5 lunar samples. *Earth and Planetary Science Letters*, *596*, 117791. https://doi.org/10.1016/j.epsl.2022.117791

Jia, Z., Chen, J., Kong, J., Qiao, L., Fu, X., & Ling, Z. (2024). Geologic context of Chang'e-6 candidate landing regions and potential non-mare materials in the returned samples. *Icarus*, *116107*, 116107. https://doi.org/10.1016/j.icarus.2024.116107

Krasilnikov, S. S., Ivanov, M. A., Head, J. W., & Krasilnikov, A. S. (2023). Geologic history of the south circumpolar region (SCR) of the Moon. *Icarus*, *394*, 115422. https://doi.org/10.1016/j.icarus.2022.115422

Le Feuvre, M., & Wieczorek, M. A. (2011). Nonuniform cratering of the Moon and a revised crater chronology of the inner Solar System. *Icarus*, *214*(1), 1–20. https://doi.org/10.1016/j.icarus.2011.03.010

Li, C., Hu, H., Yang, M. F., Liu, J., Zhou, Q., Ren, X., et al. (2024). Nature of the lunar far-side samples returned by the Chang'E-6 mission. *National Science Review*, *11*(11), nwae328. https://doi.org/10.1093/nsr/nwae328

Li, Q. L., Zhou, Q., Liu, Y., Xiao, Z., Lin, Y., Li, J. H., et al. (2021). Two-billion-year-old volcanism on the Moon from Chang'e-5 basalts. *Nature*, *600*(7887), 54–58. https://doi.org/10.1038/s41586-021-04100-2

Liu, Z. Q., Peng, M., Di, K. C., Wan, W. H., Liu, B., Wang, Y. X., et al. (2024). High-precision visual localization of the Chang'e-6 lander. *National Remote Sensing Bulletin*, *28*(6), 1649–1656. https://doi.org/10.11834/jrs.20244229

Losiak, A., Wilhelms, D., Byrne, C., Thaisen, K., Weider, S., Kohout, T., et al. (2009). A new lunar impact crater database. In *Lunar and planetary science conference* (Vol. 40). LPI. Retrieved from https://www.lpi.usra.edu/lunar/surface/

Marchi, S., Mottola, S., Cremonese, G., Massironi, M., & Martellato, E. (2009). A new chronology for the Moon and Mercury. *The Astronomical Journal*, *137*(6), 4936. https://doi.org/10.1088/0004-6256/137/6/4936

Mazrouei, S., Ghent, R. R., Bottke, W. F., Parker, A. H., & Gernon, T. M. (2019). Earth and Moon impact flux increased at the end of the Paleozoic. *Science*, *363*(6424), 253–257. https://doi.org/10.1126/science.aar4058

Melosh, H. J. (1989). *Impact cratering: A geologic process*. Oxford University Press; Oxford: Clarendon Press.

Melosh, H. J., Kendall, J., Horgan, B., Johnson, B. C., Bowling, T., Lucey, P. G., & Taylor, G. J. (2017). South Pole–Aitken basin ejecta reveal the Moon's upper mantle. *Geology*, *45*(12), 1063–1066. https://doi.org/10.1130/G39375.1

Meyer, H. M., Denevi, B. W., Robinson, M. S., & Boyd, A. K. (2020). The global distribution of lunar light plains from the lunar reconnaissance orbiter camera. *Journal of Geophysical Research: Planets*, *125*(1), e2019JE006073. https://doi.org/10.1029/2019JE006073

Miljković, K., Wieczorek, M. A., Collins, G. S., Laneuville, M., Neumann, G. A., Melosh, H. J., et al. (2013). Asymmetric distribution of lunar impact basins caused by variations in target properties. *Science*, *342*(6159), 724–726. https://doi.org/10.1126/science.1243224

Moriarty Iii, D. P., & Pieters, C. M. (2018). The character of South Pole-Aitken Basin: Patterns of surface and subsurface composition. *Journal of Geophysical Research: Planets*, *123*(3), 729–747. https://doi.org/10.1002/2017JE005364

Moriarty Iii, D. P., Watkins, R. N., Valencia, S. N., Kendall, J. D., Evans, A. J., Dygert, N., & Petro, N. E. (2021). Evidence for a stratified upper mantle preserved within the South Pole-Aitken basin. *Journal of Geophysical Research: Planets*, *126*(1), e2020JE006589. https://doi.org/10.1029/2020JE006589

Neukum, G. (1983). *Meteoritenbombardement und Datierung planetarer Oberflachen* (p. 186). Habilitation dissertation for faculty membership. Ludwig-Maximilians-University.

Neukum, G., Ivanov, B., & Hartmann, W. (2001). Cratering records in the inner solar system in relation to the lunar reference system. *Space Science Reviews*, *96*(1–4), 55–86. https://doi.org/10.1023/A:1011989004263
Neumann, G. A. (2009). Lunar orbiter laser altimeter raw data set, LRO-L-LOLA-4-GDR-V1.0 [Dataset]. *NASA Planetary Data System (PDS)*. https://doi.org/10.17189/1520642
Oberbeck, V. R., Hörz, F., Morrison, R. H., Quaide, W. L., & Gault, D. E. (1975). On the origin of the lunar smooth-plains. *The Moon*, *12*(1), 19–54. https://doi.org/10.1007/BF02626332
Orgel, C., Torres, I., Besse, S., van der Bogert, C. H., Bahia, R., Prissang, R., et al. (2024). Characterization of high-priority landing sites for robotic exploration missions in the Apollo basin, Moon. *The Planetary Science Journal*, *5*(2), 29. https://doi.org/10.3847/PSJ/ad1108
Petro, N. E., & Pieters, C. M. (2004). Surviving the heavy bombardment: Ancient material at the surface of south Pole-Aitken basin. *Journal of Geophysical Research*, *109*(E6). https://doi.org/10.1029/2003JE002182
Petro, N. E., & Pieters, C. M. (2006). Modeling the provenance of the Apollo 16 regolith. *Journal of Geophysical Research*, *111*(E9). https://doi.org/10.1029/2005JE002559
Petro, N. E., & Pieters, C. M. (2008). The lunar-wide effects of basin ejecta distribution on the early megaregolith. *Meteoritics & Planetary Sciences*, *43*(9), 1517–1529. https://doi.org/10.1111/j.1945-5100.2008.tb01025.x
Pike, R. J. (1974). Ejecta from large craters on the Moon: Comments on the geometric model of McGetchin et al. *Earth and Planetary Science Letters*, *23*(3), 265–271. https://doi.org/10.1016/0012-821X(74)90114-9
Pike, R. J. (1977). Size-dependence in the shape of fresh impact craters on the Moon. In *Impact and explosion cratering: Planetary and terrestrial implications* (pp. 489–509).
Pike, R. J. (1980). Control of crater morphology by gravity and target type-Mars, Earth, Moon. In Lunar and planetary science conference, *11th, Houston, TX, march 17-21, 1980, proceedings* (Vol. 11, pp. 2159–2189). Pergamon Press, NASA-supported research.
Potter, R. W., Head, J. W., Guo, D., Liu, J., & Xiao, L. (2018). The Apollo peak-ring impact basin: Insights into the structure and evolution of the South Pole–Aitken basin. *Icarus*, *306*, 139–149. https://doi.org/10.1016/j.icarus.2018.02.007
Qian, Y., Head, J., Michalski, J., Gong, S., Yang, W., Wang, Z., et al. (2024). Extensive intrusive magmatism in the lunar farside Apollo and south Pole–Aitken basins, Chang'e-6 landing site. *The Astrophysical Journal Letters*, *971*(2), L39. https://doi.org/10.3847/2041-8213/ad698f
Qian, Y., Head, J., Michalski, J., Wang, X., van der Bogert, C. H., Hiesinger, H., et al. (2024). Long-lasting farside volcanism in the Apollo basin: Chang'e-6 landing site. *Earth and Planetary Science Letters*, *637*, 118737. https://doi.org/10.1016/j.epsl.2024.118737
Qian, Y., Xiao, L., Head, J. W., Wöhler, C., Bugiolacchi, R., Wilhelm, T., et al. (2021). Copernican-aged (<200 Ma) impact ejecta at the Chang'e-5 landing site: Statistical evidence from crater morphology, morphometry, and degradation models. *Geophysical Research Letters*, *48*(20), e2021GL095341. https://doi.org/10.1029/2021GL095341
Qiao, L., Head, J. W., Ling, Z., & Wilson, L. (2020). Lunar irregular mare patches: Classification, characteristics, geologic settings, updated catalog, origin, and outstanding questions. *Journal of Geophysical Research: Planets*, *125*(7), e2019JE006362. https://doi.org/10.1029/2019JE006362
Qiao, L., Xu, L., Yang, Y., Xie, M., Chen, J., Fang, K., & Ling, Z. (2021). Cratering records in the Chang'e-5 mare unit: Filling the "age gap" of the lunar crater chronology and preparation for its recalibration. *Geophysical Research Letters*, *48*(22), e2021GL095132. https://doi.org/10.1029/2021GL095132
Robbins, S. J. (2014). New crater calibrations for the lunar crater-age chronology. *Earth and Planetary Science Letters*, *403*, 188–198. https://doi.org/10.1016/j.epsl.2014.06.038
Robbins, S. J. (2019). A new global database of lunar impact craters> 1–2 km: 1. Crater locations and sizes, comparisons with published databases, and global analysis. *Journal of Geophysical Research: Planets*, *124*(4), 871–892. https://doi.org/10.1029/2018JE005592
Robinson, M. (2009). LRO Moon LROC 2 EDR V1.0 [Dataset]. *NASA Planetary Data System (PDS)*. https://doi.org/10.17189/1520250
Robinson, M. S., Brylow, S. M., Tschimmel, M. E., Humm, D., Lawrence, S. J., Thomas, P. C., et al. (2010). Lunar reconnaissance orbiter camera (LROC) instrument overview. *Space Science Reviews*, *150*(1–4), 81–124. https://doi.org/10.1007/s11214-010-9634-2
Spohn, T., Breuer, D., & Johnson, T. (Eds.) (2014)., *Encyclopedia of the solar system*. Elsevier.
Stöffler, D., & Ryder, G. (2001). Stratigraphy and isotope ages of lunar geologic units: Chronological standard for the inner solar system. *Space Science Reviews*, *96*(1), 9–54. https://doi.org/10.1023/A:1011937020193
Sun, L., & Lucey, P. G. (2024). Lunar mantle composition and timing of overturn indicated by Mg# and mineralogy distributions across the South Pole-Aitken basin. *Earth and Planetary Science Letters*, *643*, 118931. https://doi.org/10.1016/j.epsl.2024.118931
Tartèse, R., Anand, M., Gattacceca, J., Joy, K. H., Mortimer, J. I., Pernet-Fisher, J. F., et al. (2019). Constraining the evolutionary history of the Moon and the inner solar system: A case for new returned lunar samples. *Space Science Reviews*, *215*(8), 54. https://doi.org/10.1007/s11214-019-0622-x
Wang, Y., Xie, M., Xiao, Z., & Cui, J. (2020). The minimum confidence limit for diameters in crater counts. *Icarus*, *341*, 113645. https://doi.org/10.1016/j.icarus.2020.113645
Xie, M., Liu, T., & Xu, A. (2020). Ballistic sedimentation of impact crater ejecta: Implications for the provenance of lunar samples and the resurfacing effect of ejecta on the lunar surface. *Journal of Geophysical Research: Planets*, *125*(5), e2019JE006113. https://doi.org/10.1029/2019JE006113
Xie, M., Xiao, Z., Xu, L., Fa, W., & Xu, A. (2021). Change in the Earth–Moon impactor population at about 3.5 billion years ago. *Nature Astronomy*, *5*, 128–133. https://doi.org/10.1038/s41550-020-01241-8
Xie, M., Xiao, Z., Zhang, X., & Xu, A. (2020). The provenance of regolith at the Chang'e-5 candidate landing region. *Journal of Geophysical Research: Planets*, *125*(5), e2019JE006112. https://doi.org/10.1029/2019JE006112
Xie, M., & Zhu, M. H. (2016). Estimates of primary ejecta and local material for the Orientale basin: Implications for the formation and ballistic sedimentation of multi-ring basins. *Earth and Planetary Science Letters*, *440*, 71–80. https://doi.org/10.1016/j.epsl.2016.02.012
Xu, L. (2024). Crater catalogue for age determination of the Chang'e-6 mare unit and key ejecta source craters (v1.0) [Dataset]. *Zenodo*. https://doi.org/10.5281/zenodo.13932641
Xu, L., & Xie, M. (2020). Ejecta thickness distribution of the Schrödinger basin on the Moon. *Journal of Geophysical Research: Planets*, *125*(12), e2020JE006506. https://doi.org/10.1029/2020JE006506
Xu, L., Zhang, X., Qiao, L., & Lai, J. (2021). Evaluating the thickness and stratigraphy of ejecta materials at the Chang'E-4 landing site. *The Astronomical Journal*, *162*(1), 29. https://doi.org/10.3847/1538-3881/abf8b0
Yang, C., Zhang, X., Bruzzone, L., Liu, B., Liu, D., Ren, X., et al. (2023). Comprehensive mapping of lunar surface chemistry by adding Chang'e-5 samples with deep learning. *Nature Communications*, *14*(1), 7554. https://doi.org/10.1038/s41467-023-43358-0
Yang, W., Chen, Y., Wang, H., Tian, H.-C., Hui, H., Xiao, Z., et al. (2022). Geochemistry of impact glasses in the Chang'e-5 regolith: Constraints on impact melting and the petrogenesis of local basalt. *Geochimica et Cosmochimica Acta*, *335*, 183–196. https://doi.org/10.1016/j.gca.2022.08.030

Yue, Z., Di, K., Wan, W., Liu, Z., Gou, S., Liu, B., et al. (2022). Updated lunar cratering chronology model with the radiometric age of Chang'e-5 samples. *Nature Astronomy*, *6*(5), 541–545. https://doi.org/10.1038/s41550-022-01604-3

Yue, Z., Gou, S., Sun, S., Yang, W., Chen, Y., Wang, Y., et al. (2024). Geological context of the Chang'e-6 landing area and implications for sample analysis. *The Innovation*, *5*(5), 100663. https://doi.org/10.1016/j.xinn.2024.100663

Zeng, X., Liu, D., Chen, Y., Zhou, Q., Ren, X., Zhang, Z., et al. (2023). Landing site of the Chang'e-6 lunar farside sample return mission from the Apollo basin. *Nature Astronomy*, *7*(10), 1188–1197. https://doi.org/10.1038/s41550-023-02038-1

Zhang, X. (2023). lunar_surface_chemistry_maps [Dataset]. *figshare*. https://doi.org/10.6084/m9.figshare.24081438.v50

Zhou, C., Jia, Y., Liu, J., Li, H., Fan, Y., Zhang, Z., et al. (2022). Scientific objectives and payloads of the lunar sample return mission—Chang'E-5. *Advances in Space Research*, *69*(1), 823–836. https://doi.org/10.1016/j.asr.2021.09.001

Zong, K., Wang, Z., Li, J., He, Q., Li, Y., Becker, H., et al. (2022). Bulk compositions of the Chang'E-5 lunar soil: Insights into chemical homogeneity, exotic addition, and origin of landing site basalts. *Geochimica et Cosmochimica Acta*, *335*, 284–296. https://doi.org/10.1016/j.gca.2022.06.037

References From the Supporting Information

Fassett, C. I., & Thomson, B. J. (2014). Crater degradation on the lunar maria: Topographic diffusion and the rate of erosion on the Moon. *Journal of Geophysical Research: Planets*, *119*(10), 2255–2271. https://doi.org/10.1002/2014JE004698

Ghent, R. R., Hayne, P. O., Bandfield, J. L., Campbell, B. A., Allen, C. C., Carter, L. M., & Paige, D. A. (2014). Constraints on the recent rate of lunar ejecta breakdown and implications for crater ages. *Geology*, *42*(12), 1059–1062. https://doi.org/10.1130/G35926.1

Greeley, R., Kadel, S. D., Williams, D. A., Gaddis, L. R., Head, J. W., McEwen, A. S., et al. (1993). Galileo imaging observations of lunar maria and related deposits. *Journal of Geophysical Research*, *98*(E9), 17183–17205. https://doi.org/10.1029/93JE01000

Haruyama, J., Hara, S., Hioki, K., Iwasaki, A., Morota, T., Ohtake, M., & Iwata, T. (2012). Lunar global digital terrain model dataset produced from SELENE (Kaguya) terrain camera stereo observations. In *43rd annual lunar and planetary science conference* (Vol. 1659, p. 1200).

Kneissl, T., van Gasselt, S., & Neukum, G. (2011). Map-projection-independent crater size-frequency determination in GIS environments—New software tool for ArcGIS. *Planetary and Space Science*, *59*(11–12), 1243–1254. https://doi.org/10.1016/j.pss.2010.03.015

Michael, G. G., & Neukum, G. (2010). Planetary surface dating from crater size–frequency distribution measurements: Partial resurfacing events and statistical age uncertainty. *Earth and Planetary Science Letters*, *294*(3–4), 223–229. https://doi.org/10.1016/j.epsl.2009.12.041

Pasckert, J. H., Hiesinger, H., & van der Bogert, C. H. (2018). Lunar farside volcanism in and around the South Pole–Aitken basin. *Icarus*, *299*, 538–562. https://doi.org/10.1016/j.icarus.2017.07.023

Soderblom, L. A. (1970). A model for small-impact erosion applied to the lunar surface. *Journal of Geophysical Research*, *75*(14), 2655–2661. https://doi.org/10.1029/JB075i014p02655

Wang, Y., Xie, M., Xiao, Z., & Cui, J. (2020). The minimum confidence limit for diameters in crater counts. *Icarus*, *341*, 113645. https://doi.org/10.1016/j.icarus.2020.113645

Xie, M., Zhu, M. H., Xiao, Z., Wu, Y., & Xu, A. (2017). Effect of topography degradation on crater size-frequency distributions: Implications for populations of small craters and age dating. *Geophysical Research Letters*, *44*(20), 10171–10179. https://doi.org/10.1002/2017GL075298

Xu, L., Qiao, L., Xie, M., & Wu, Y. (2022). Formation age of lunar Lalande crater and its implications for the source region of the KREEP-rich meteorite Sayh al Uhaymir 169. *Icarus*, *386*, 115166. https://doi.org/10.1016/j.icarus.2022.115166